UNIVERSITAT POLITÈCNICA DE VALÈNCIA

UNIVERSITAT POLITÈCNICA DE VALÈNCIA

Escuela Técnica Superior de Ingeniería Industrial

Accessory Pathway Localisation Optimisation In Silico Heart Model

Trabajo Fin de Grado

Grado Universitario en Ingeniería Biomédica

AUTOR/A: Martí Roig, Adrián

Tutor/a: Millet Roig, José Pock, Thomas

CURSO ACADÉMICO: 2023/2024

Accessory Pathway Localisation Optimisation In Silico Heart Model

Adrian Marti Roig

Institute of Computer Graphics and Vision
Graz University of Technology, Austria

Bachelor Thesis
Dr. Thomas Pock
Graz, August 24, 2024

Abstract

Wolff-Parkinson-White (WPW) syndrome is a cardiovascular disease characterized by abnormal atrio-ventricular conduction facilitated by accessory pathways (APs). The primary treatment modality is invasive catheter ablation of the AP. Successful ablation outcomes depend on precise localization of the APs; however, current catheter diagnostic procedures often struggle with accurately determining AP locations. In order to gain insight into how a high density mapping catheter can be used to locate an AP, a virtual cardiac model is employed.
A cardiac model of electrophysiology that was specifically tailored to represent antegrade APs in the form of a short atrio-ventricular bypass tract was utilised. An HD-Grid catheter model was laid over the ventricular endocardial surface of the model to obtain EGMs near the AP ending point. The retrieved unipolar EGMs where used to compute bipolar EGMs, omnipolar EGMs and vector maps. The computed bibolars were compared with real bipolar EGMs, showing clear resemblance.
The findings highlight the potential of this new tool as a foundation for further research over optimal ablation sites localisation and cardiac mapping in general. Moreover, it will not only deepen our understanding of the underlying mechanisms of WPW syndrome but also potentially enhance the diagnostic accuracy of cardiac mapping procedures.

Keywords: *Wolff-Parkinson-White Syndrome, Accessory Pathways, Electrograms, High Density Mapping, Virtual Models of Cardiac Electrophysiology*

Contents

1 Introduction

Wolff-Parkinson-White (WPW) syndrome is a heart rhythm disorder that is characterised by the presence of at least one or more accessory pathways (APs) facilitating abnormal atrio-ventricular conduction. WPW typically manifests in children and affects between 0.68 and 1.7 in 1000 in the general population [4]. Without treatment, the condition can lead to paroxysmal palpitations and morbidity through supraventricular tachycardias or sudden cardiac arrest [5]. Treatment of WPW syndrome typically involves invasive catheter ablation in efforts to restore the normal heart rhythm. Catheter ablation is a procedure in which hot or cold energy is used to create tiny scars, targeting in this case the AP, to render the tissue electrically inactive. However, approximately 6% of ablations in WPW are still unsuccessful [15].

From a clinical perspective, accurate prediction of the location of an AP is of great value as it relates to procedural planning, risk prediction, and procedural outcome [2]. The position of the AP can be detected prior to the procedure using localisation algorithms that rely on the clinically standard 12-lead electrocardiogram (ECG) [24, 30, 25, 39]. Prediction accuracy is fairly high at above 90% for most recent techniques [3]. However, such algorithms are known to be less sensitive in the septum, deep coronary sinus, and in close proximity to the His-bundle. The algorithms are also not applicable in the instance when the patient has a compounding condition such as atrial fibrillation, ventricular tachycardia, or myocardial infraction.

When pre-procedural localisation fails, electro-antomical mapping of the endocardium of the heart is used to localise the AP during the procedure. High Density (HD) Mapping catheters, like the HD-Grid from Abbott, offer enhanced local electrical conduction and depolarisation wavefront characterisation by having a lot of recording electrodes packed in a small area, each of those, measuring the electrograms (EGMs). Furthermore, they offer the possibility of retrieving a completely new set of parameters, like local vector maps or the vector field heterogeneity, that may help to locate APs.

Since obtaining on-demand signals in-vivo is not feasible, as real heart tissues for research are scarce and obtaining them involves invasive procedures, an exploration in-vitro is needed. Computational heart models are a strong tool that enables researchers and medical professionals to extensively explore the complexities of the human heart without the ethical and practical issues associated with using real human hearts. One of the main advantages of using computer-based heart models is the ability to simulate various scenarios and conditions in a controlled, virtual environment, that would be impossible to reproduce in a real heart. This capability is invaluable for planning complex surgeries, thereby enhancing the precision and safety of medical interventions.

Virtual models of cardiac electrophysiology (EP) that are capable of representing WPW syndrome can be of value in order to undersand how HD-grid mapping can be used to better localise the pathway. These EP models are becoming increasingly feasible for exploring the mechanisms behind various cardiac diseases, serving as clinical tools, and generating data to supplement clinical data for machine learning approaches [37]. This research sits on top of previous work, where a fully detailed virtual model of WPW syndrome had been developed [19].

Therefore, this virtual model of WPW syndrome is going to be used in this research in order to gain more knowledge about APs and how can they be localised. This will be achieved using a virtual model of HD-Grid to obtain EGM signals from the endocardial ventricular surface and extracting parameters from the heart model, in order to enable accurate ablation in future interventions.

2 Background

The normal electrical conduction in the heart starts in the sino-atrial node, when it releases an electrical stimulus that passes through the myocardial cells of the atria creating a wave of

contraction which spreads rapidly through both atria. This electrical stimulus eventually reaches the atrio-ventricular node and is delayed briefly so that the contracting atria have enough time to pump all the blood into the ventricles. It is important to state that the electrical stimulus does not propagate from the atria directly to the ventricles due to an electrical isolation layer that exists between these two. When the electrical stimulus passes through the atrio-ventricular node, it goes into the His-Bundle of the His-Purkinje System (HPS) until it reaches the cells in the ventricle myocardium. These cells then contract and the ventricles pump blood out of the heart [33]. The complete electrical conduction can be seen in Figure 1A.

In the case of WPW syndrome, an abnormal extra electrical pathway, termed an AP, exists between the atria and the ventricles in the heart disrupting normal sinus rhythm. The AP allows conduction outside of the normal conduction system through the atrio-ventricular node and the His-Bundle. As shown in Figure 1B, this abnormal conduction can lead both to orthodromic or antidromic conduction. WPW syndrome is a common clinical disorder affecting up to 2.0% of the population leading to paroxysmal palpitations and morbidity through supraventricular tachycardias or sudden cardiac arrest [6].

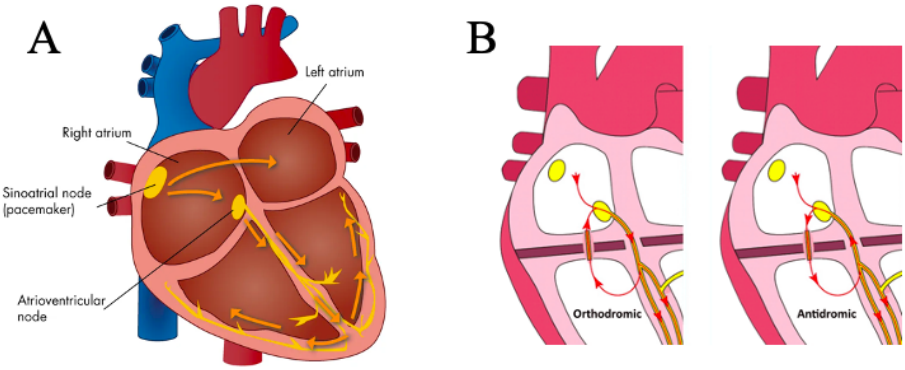

Figure 1: Normal electrical conduction of the heart (A) and abnormal electrical conduction caused by an AP (B)

The contraction that occur in the cells of the tissue to pump the blood is called depolarisation. Afterwards comes the repolarisation of the cells, which is the process allowing them to regain their ability to depolarise and contract again. Both steps are mediated by the change of the membrane voltage, or potential across the cell membrane, which is determined at any time by the relative ratio of ions, extracellular to intracellular [28]. This change in the membrane potential is known as the action potential of the cell, represented in Figure 2. The resting membrane potential is around -90 mV, it rises when the cell depolarises and it returns to its resting value when the repolarisation occurs.

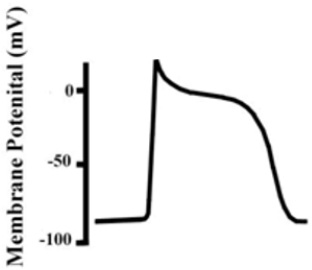

Figure 2: Usual membrane action potential that can be measured from a heart cell. It occurs due to the change in the ratio of ions between the inside and the outside of the cell. From [40]

2.1 Accessory Pathway Localisation

EGMs are signals generated by the potential (voltage) differences recorded at two recording electrodes during the cardiac cycle. There are two types of EGM signals –unipolar and bipolar– each with unique properties as showcased in Figure 3A. Unipolar cardiac EGMs are obtained by positioning the exploring electrode in the heart and the second electrode distant from the heart such that it has little or no cardiac signal [41]. Morphology in these signals indicate the direction of wavefront propagation. However, unipolar EGMs can contain substantial far-field signal generated by depolarisation of tissue remote from the recording electrode, obscuring the small local potentials. Therefore, unipolar potentials are generally always filtered to remove far-field noise.

Bipolar recordings, on the other hand, are obtained by connecting two electrodes that are exploring the area of interest to the recording amplifier, as seen in Figure 3B. At each point in time, the potential generated is the sum of the potential from the positive input and the potential at the negative input. The potential at the negative input is subtracted from the one at the positive input. Because the far-field signal is similar at each instant in time, it is largely subtracted out, leaving only the local signal [41]. Bipolar recordings are used to locate focal arrhythmias by identifying the point of earliest activation relative to a stable reference. Moreover, reducing the amplitude of the far-field signal facilitates identification of local depolarisation in abnormal areas of infarction or scar in bipolar recordings.

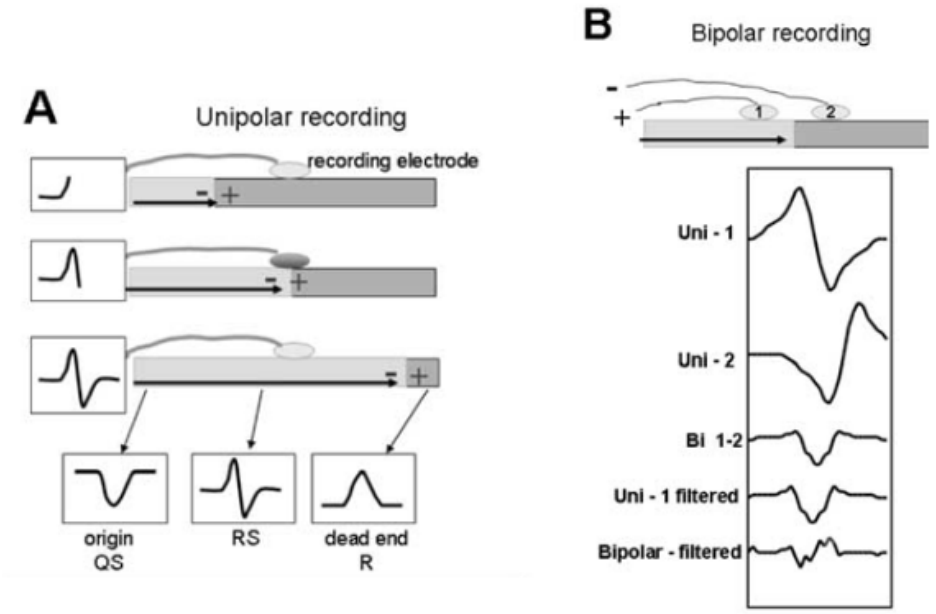

Figure 3: Generation of unipolar and bipolar EGMs. The horizontal bars at the top of figures A and B represent a sheet of myocardium with depolarisation propagating from left to right (arrow). Electrodes resting on the tissue are shown as grey circles. Unipolar recording is shown in A. Theoretical EGMs are shown in boxes. B shows bipolar recording. Electrode 2 is subtracted from electrode 1. Electrograms created by a mathematical simulation are shown below the schematic. Compared to the signal from electrode 1 (Uni-1), the signal from electrode 2 (Uni-2) is slightly delayed (because the wavefront reaches it later) and is inverted because it is going to be subtracted. Adding these two signals together generates the bipolar signal (Bi 1–2) that removes much of the far-field signal. Differentiating the Uni-1 signal decreases the far-field component and produces a signal quite similar to the bipolar signal but slightly shifted with respect to time. Differentiating the bipolar signal produces additional deflections and further complicates the signal. From [41].

Bipolar recordings are preferred over unipolar for catheter mapping in humans and particularly for scar-related arrhythmias. In contrast to unipolar recordings, the amplitude of a bipolar electrogram is influenced by the direction of wavefront propagation. A wavefront that is prop-

agating in the direction exactly perpendicular to the axis of the recording dipole produces no difference in potential between the electrodes, and hence no signal.

Due to their characteristics, bipolar EGMs are used for locating APs, by looking for the location where a Kent potential appears. This Kent potential is a sharp, rapid deflection preceding the onset of ventricular activation, as Figure 4 shows. However successful localisation and catheter ablation of APs in patients with WPW syndrome during atria fibrillation has not yet been reported [16].

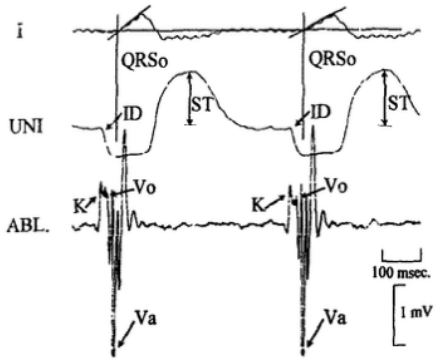

Figure 4: Standard lead I of the surface ECG, unfiltered unipolar EGM (UNI) recorded from the tip electrode of the ablation catheter and bipolar EGM (ABL). Shown by an arrow is the Kent potential (K) with its characteristic rapid deflection preceding the onset of ventricular activation (Va). From [16].

Furthermore, this AP's potential is not always dissociated from local atrial or ventricular activation and, when detected, it not always leads to a successful ablation on that site [42]. Therefore doctors still lack of precise indicators for locating APs often causing excessive tissue ablation.

2.2 High Density Mapping and New Parameters

High Density (HD) Mapping catheters like the HD-Grid from Abbott try to solve these problems by characterising local electrical conduction. The HD-Grid consists in a 2D array of 4x4 electrodes, 16 in total. Each electrode is a 1mmx1mm square and is separated by 3mm from the beyond electrodes, like Figure 5 shows.

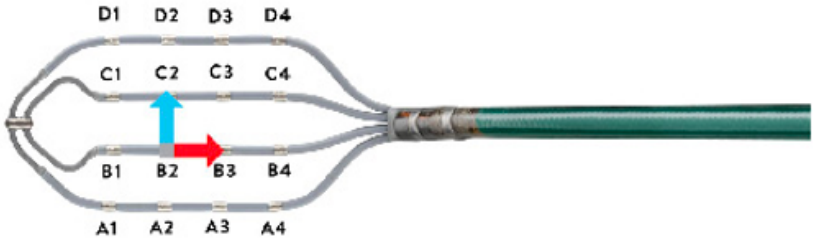

Figure 5: Advisor HD Grid. From [34].

This type of catheter performs cardiac mapping, a rapidly expanding field that helps depict the heart's electrical activity, anatomy and tissue characteristics in real-time, that helps cardiologists during procedures [34]. Furthermore, HD catheters can be used to obtain omnipolar EGMs, which are calculated within a clique, that is defined as a square of four electrodes (see Figure 6) [7].

Omnipoles are bipole-like, catheter orientation independent signals which use characteristics of a locally propagating depolarisation wavefront. Within a clique, omnipolar EGMs allow us to mathematically obtain bipolar EGMs in any direction without physically rotating a sensing

electrode [14]. This directly enables visualisation of wavefronts on a mapping catheter and constitutes our concept of a new mapping strategy [11].

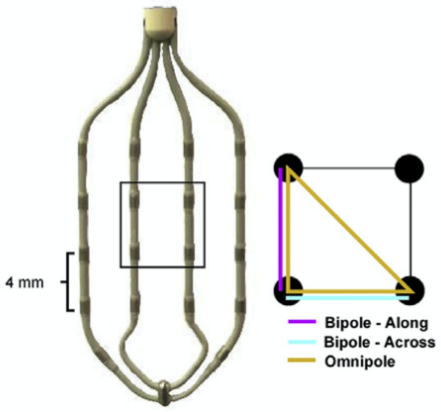

Figure 6: Clique in the advisor HD Grid. The bipolar orientations are shown in magenta and cyan. The clique of electrodes used to calculate omnipolar electrograms (yellow triangle) are also shown. From [13].

High Density mapping also allows us to get more parameters regarding the electrical activation of the tissue. Local activation timing maps are used to represent by colours, the time when the tissue from a certain location of the HD-Grid has been activated (Figure 7A). This allows cardiologists have a glimpse of how the tissue is being activated, and it has already been used in some procedures [26]. It is also possible to calculate local vector maps (Figure 7B), that represent the propagation direction of the wavefront within each clique, and the vector field heterogeneity (Figure 7C), designed to quantify the heterogeneity of propagation wavefronts in local vector maps derived from omnipolar EGMs [36]. These are some different parameters that are possible to calculate to potentially find a measure that helps doctors locate APs.

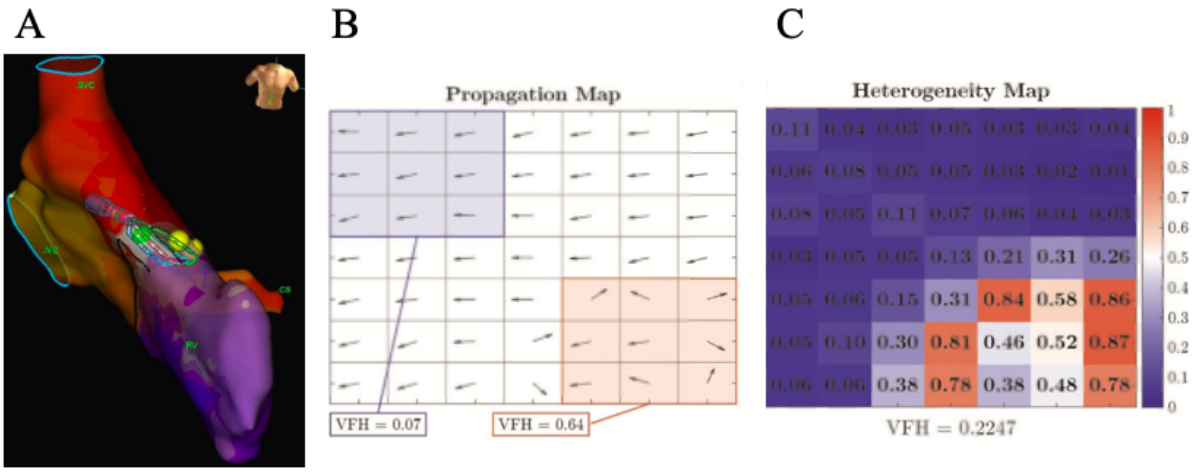

Figure 7: Local activation timing map during a procedure shown on A. On B, local vector map obtained with a multielectrode mapping catheter with 128 electrodes from rabbit hearts is shown. C shows the vector field heterogeneity (VFH) computed on the same signals as in B. In can be seen that the higher the differences between the propagation direction on a region, the higher the heterogeneity value. From [26, 36].

Using the advantages that the HD-Grid gives to cardiologists, Casado R, et al, already reported a successful ablation using this new catheter [10], that helped him to identify the trajectory of the AP and locating it. However, he was looking for the point where the Kent potential was expressed, only looking at bipolar EGMs. Yet the localisation of the Kent potential has not been proved to work every time, as has been stated above.

Other studies such as [12] only looked for the point where the shortest ventriculoatrial conduction time and the earliest ventricular potential were detected. They used a quadripolar catheter and looked only to unipolar and bipolar EGMs, having more success than other studies. However, a better localisation of APs can be achieved with the possibilities that the HD-Grid yields.

2.3 Cardiac EP Model

Previous research involved constructing a detailed model of whole-heart electrophysiology from clinical magnetic resonance images. This model is customised for an individual subject according to clinically-recorded 12 lead ECGs in order to simulate a realistic normal sinus rhythm [20]. It includes a more physiologically-detailed representation of the HPS, developed in [21] and a the possibility to model WPW syndrome by introducing an AP as done in [19]. Atrial EP is then accounted for and delayed atrio-ventricular conduction is allowed through an atrio-ventricular node located at the base of the right atrium connected to the HPS.

Very few virtual technologies simulating the entire organ-scale EP of all four-chambers of the heart have been reported and widespread clinical use is limited due to high computational costs and difficulty in validation. However, this novel virtual technology of representing the EP of all four-chambers of a virtual heart is aimed to overcome these limitations. It has been validated through phantom validation (that the phantom closely represents the real anatomy and function of the system being studied) [27] and through signal validation (that the ECG and the EGMs are similar to the real data)[22]. This ensures that the model is physiological, reliable and predictive. Moreover, its completeness is demonstrated in [22] by modeling two pathologies of the cardiac conduction system, left bundle branch block and right bundle branch block, the model was not parameterised for, being able to replicate intricate morphological features of the 12 lead ECG during both normal sinus rhythm, as well as during these two pathologies. In the same research it is also stated that the model can be used under scenarios to which it was not calibrated for, without the need of model re-fitting. Furthermore, not only is the model capable of predicting non-invasive data acquired in clinical routine, but also invasive measurements as acquired during an intervention, like EGMs.

2.4 Universal Ventricular and Atrial Coordinates

To automatically control and adjust parameters of the EP, as well as to introduce an AP and select specific locations in the heart, the model has been equipped with an abstract reference frame. This frame includes both universal ventricular coordinates (UVCs) [18] and universal atrial coordinates (UACs) [35], allowing for precise manipulation and customisation of the model. These coordinates are used to describe position within any heart as UVCs and UACs comprise four unique coordinates that have been chosen to be intuitive, well defined, and relevant for physiological descriptions. Furthermore, they also help in automatic registration of imaging, automatic registration of electro-anatomical mapping data, 2D visualisation, and patient specific model creation. On the one hand, the UVCs are defined as follows:

- Apicobasal coordinate, ζ (Figure 8A). Its value is between 0 and 1, with 0 being the apex and 1 being the base of the heart. and it represents the distance traveled along the long axis of the ventricles from the apex to the base.
- Transmural coordinate, ρ (Figure 8B). It represents the transmurality, that is the distance from the endocardium (innermost layer of the heart) to epicardium (outermost layer of the heart). Its minimum value is 0, corresponding to the endocardium; and its maximum value is 1, corresponding to the epicardium.
- Rotational coordinate, ϕ (Figure 8C). It represents the circumferential rotation around the long axes of the left ventricle (LV) and right ventricle (RV). In the LV, ϕ rotates from

0 to $+2\pi$ starting in the middle of the septum. In the RV, the ϕ coordinate rotates from $+\pi/2$ at the anterior surface of the LV-RV junction to $\pi/2$ at the posterior surface of the LV-RV junction.

- Transventricular coordinate, ν (Figure 8D). It determines whether the other three coordinates are within the LV or RV of the mesh. This coordinate only takes two values, 0 for the LV and 1 for the RV.

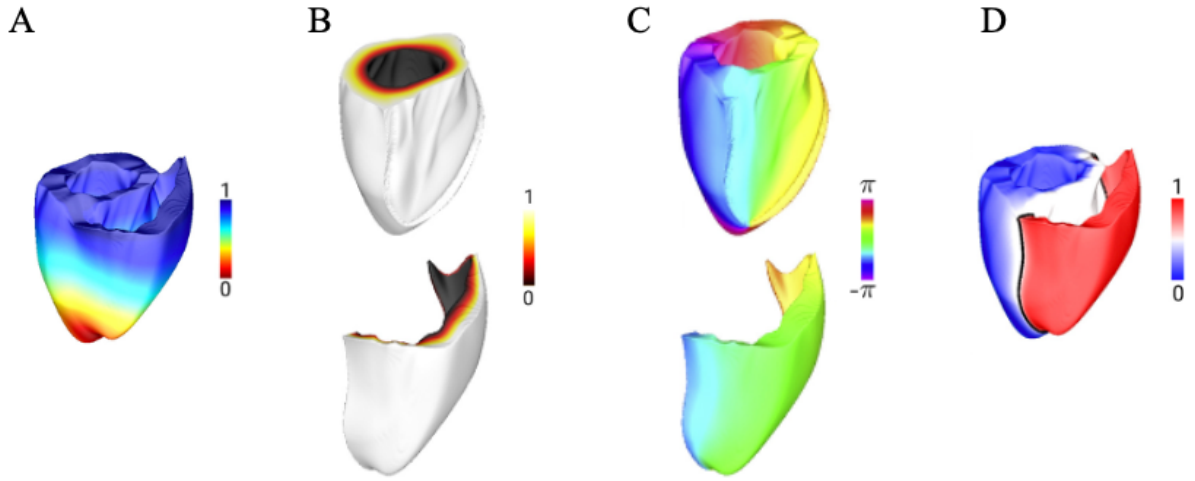

Figure 8: UVC system: apicobasal coordinate (A), transmural coordinate (B), rotational coordinate (C) and transventricular coordinate (D). From [18].

On the other hand, the UACs are more challenging to define due to their more complex shape. The transmural coordinate and the transventricular coordinate (transatrial coordinate in this case) are the same as in UVCs. However, two new coordinates are defined:

- Septal-lateral coordinate, α. In the left atria (LA), it is constructed between the mitral valve (MV) and the junctions of each of the superior veins with the LA body (Figure 9B). In the righ atria (RA), it is constructed between the tricuspid valve (TV) and the junctions of the superior and inferior vena cava with the RA body (Figure 9A).

- Posterior-anterior coordinate, β. In the LA, it is constructed between the MV and the path between the junction of the right and left superior pulmonary veins with the LA (Figure 9B). In the RA, it is constructed between the tricuspid valve (TV) and the path between the junctions of the superior and inferior vena cava with the RA (Figure 9A).

3 Methods

A model of WPW assuming antegrade AP conduction was first generated within a pre-existing model. An HD-Grid model with the possibility to map any location on the endocardial ventricular surface was constructed. To prove that signals generated on the simulation can be extracted with the HD-Grid model, bipolar EGMs and vector maps were computed.

3.1 Accessory Pathway Representation

The method developed in [19] is used to generate APs in different locations of the heart. This method only needs the atrial coordinates of the starting point of the AP in the atria and the

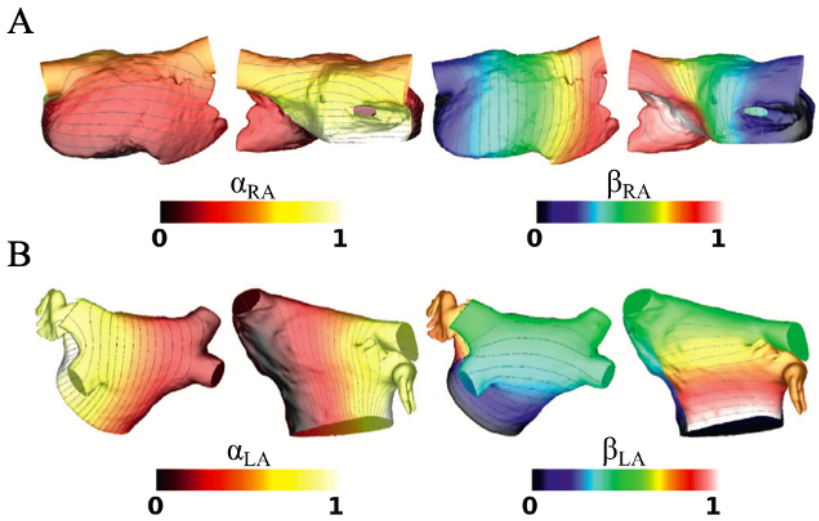

Figure 9: UAC system: A shows the septal-lateral (left) and the posterior-anterior coordinates (right) in RA, whereas B shows the septal-lateral (left) and the posterior-anterior (right) coordinates in LA. From [35].

vetricular coordinates of its ending point in the ventricles. A short atrio-ventricular bypass tract allowing antegrade conduction is then inserted within the model allowing abnormal conduction from the atria to the ventricles and facilitating pre-ventricular excitation. A realistic conduction velocity of $2.0ms^{-1}$ is set to replicate His-Purkinje fibers in accordance with reported conduction velocities in Mahaim Accessory Pathways [38].

3.2 Electrical Activity Simulation

In order to simulate the electrical activity of the heart once the AP has been introduced, the Reaction-Eikonal (R-E) model is used [31]. The R-E model combines the computational efficiency of the eikonal model [23] with the detailed biophysical accuracy of the more computationally complex reaction–diffusion (R-D) model [32]. As proved in [31], the R-E model predicts extracellular potential fields and electrograms with high fidelity and offers vast computational savings greater than three orders of magnitude.

The R-D formulation is rooted in the bidomain model that is a mathematical representation describing the spread of cardiac electrical activity in the cardiac tissue by considering it as two interpenetrating continuous domains: the intracellular (inside the cells) and the extracellular (outside the cells) spaces. The coupling of the two domains is performed via non-linear models describing the current flow through the cell membrane, which leaves one domain to enter the other [9]. The bidomain equations state that transmembrane currents, I_m, that enter intracellular and extracellular spaces by crossing the cell membrane, represent sources for intracellular, ϕ_i, and extracellular, ϕ_i, potentials. This model takes into account a lot of parameters, such as the intracellular and extracellular conductivity tensors (σ_i and σ_e, respectively) and the membrane capacitance among others. $Vm = \phi_i\phi_e$ will be the transmembrane voltage. The full bidomain model thus provides the most physiologically-realistic representation of cardiac bioelectric activity at the organ scale, yielding Vm and ϕ_e at every point in space and time [31]. A pseudo-bidomain model approximates a full-blown bidomain model with high accuracy, but at a fraction of the computational costs. This model assumes that the intra- and extracellular domains are both anisotropic, but to the same degree, that is, $\sigma_e = \lambda\sigma_i$ holds with λ being a scalar. Thus, the bidomain equations can be reduced and simplified.

The eikonal model is added onto the R-D formulation as an efficient way of computing arrival times of depolarisation wavefronts in the myocardium. This model uses the velocity tensor $(V(x))$, σ_i and σ_e to calculate $t_a(x)$, with is a positive function describing the wavefront arrival

time at location x. It can be computed efficiently with sufficient accuracy at a lower spatial resolution and lower computational cost as compared to R-D models, which demand higher spatial resolutions. This motivates an R-E model, where the propagation of depolarisation wavefronts is mediated by eikonal-based activation maps and not by diffusion. Depolarisation at site x is initiated at time $t_a(x)$ by a prescribed stimulus current, $Ifoot$, which is designed to depolarise and activate the local membrane at x [31].

3.3 Repolarisation

The WPW syndrome model also has to model the repolarisation of the heart tissue, once it has depolarised. It is important in order to extract real EGMs. Also, it can be of interest to model the syndrome as it occurs in patients, with the reentry arrhythmia shown in Figure 1B, where the electrical impulse goes from atria to ventricles without any pace or control.

Therefore, repolarisation is also used in R-E and is dictated by gradients in action potential duration. Action potential duration is typically defined as the time it takes for the cell to recover back 90% to the resting membrane potential after activation. This duration typically depends on cellular dynamics across various potassium channels. Within this study, we used the Mitchell-Schaeffer ionic model [29], which is a phenomenological model that does not rely on actual physical representations of ion channels and currents. Instead, there is a direct relationship between the parameter τ_{close} and the action potential duration.

The heart model that is used in this research is then capable of representing the AP and to successfully simulate the electrophysiological activity of the heart, by using both the reaction-eikonal formulation with the pseudo-bidomain model for the depolarisation and the Mitchell-Schaeffer ionic model for the repolarisation.

3.4 HD-Grid Model

With the previously described methods, the EP model is able to faithfully simulate a complete cardiac cycle (depolarisation and repolarisation). In order to retrieve the signals generated by the simulation as a real HD-Grid would do, a modeled HD-Grid is needed. The developed method on this research is able to lay over the endocardial ventricular surface a modeled HD-Grid catheter based only on an initial coordinate given in the UVC system and a direction vector for the orientation of the catheter. Moreover, as the heart is modeled in a cartesian coordinate system, each node in the mesh has an exact xyz coordinate.

In general, the HD grid is constructed from a first node of the mesh and calculating the rest of the points given an orientation direction by doing calculations of the distance from the fist point to the rest of the nodes in the mesh. The selection of the HD-Grid points is clinically viable as it is done automatically. The EGM extraction is done by basic interpolation using the finite element method.

The novel framework is able to obtain the EGM signals from any point on the endocardial ventricual surface. The simulation framework is implemented within CARP*entry* [9] and the *open*CARP simulation environment [17].

The exact algorithm performs a series of steps in order to build the HD-Grid:

1. Run a simulation of the heart activation taking into consideration the AP. For each node in the mesh, a signal of the potential variation over time is obtained. This are the unipolar EGMs.

2. Extract the endocardial surface of the ventricle in study, by selecting only some specific elements (triangles) of the mesh.

3. The exact localisation of the first point of the electrode (A1 on Figure 5), given in UVCs, into an existing node in the mesh is facilitated through open-source meshtool [1].

4. Run an eikonal simulation on the extracted endocardial surface, starting from A1. The parameters of this simulation are set to have an isotropic propagation through the surface and to have a conduction velocity of 1m/s. With this technique, exact distances from that point to the rest of the nodes in the mesh are obtained.

5. Thus with the initialised direction vector (d in Figure 10), it is possible now to select the element of the mesh that is at $\sqrt{12^2 + 12^2}$mm from A1 and contains D4 (see Figure 5). It would not be accurate to select another node of the mesh, because the HD-Grid would be deformed, so D4 will be located somewhere inside the selected element. The process to obtain the coordinates of D4 is explained with the following formulas and supported by Figure 10. Each node in the figure (n_0, n_1 and n_2) has associated its Cartesian coordinates (v_0, v_1 and v_2) and the value of its distance from A1 (e_0, e_1 and e_2).

$$e_d = \sqrt{12^2 + 12^2} \tag{1}$$

$$v_{p1} = v_0 + t_{p1}(v_2 - v_0) \tag{2}$$

$$v_{p2} = v_1 + t_{p2}(v_2 - v_1) \tag{3}$$

$$t_{p1} = \frac{e_d - e_0}{e_2 - e_0} \tag{4}$$

$$t_{p2} = \frac{e_d - e_1}{e_2 - e_1} \tag{5}$$

   Where e_d is the exact distance from A1 to D4 and v_{p1} and v_{p2} are the exact coordinates of the points p_1 and p_2. t_{p1} and t_{p2} are values between 0 and 1, and for the specific example in Figure 10, if calculated between n_0 and n_1, its value will be outside of those ranges.

6. Once p_1 and p_2 have been calculated, the intersection point (D4) between the line that joints them and d is computed.

7. Run another eikonal simulation with 3 starting points with the same characteristics as in step 4. The 3 starting points are each node that defines the element obtained in step 5. The simulation starts from a node of those 3, at a certain time based on the distance from the point D4 to the node. If D4 is closer to one node of the element, the eikonal simulation starts earlier from it that from the other two nodes. This results in data containing the exact distances from D4 to every node in the mesh.

8. Points A4 and D1 (see Figure 5) are obtained from the data in both eikonal runs, selecting the elements that are at 12mm from A1 and D4. To obtain the exact coordinates of A4 and D1, the formulas described in step 5 are again used.

9. Two more eikonal simulations are performed from A4 and D1 with the same method as in step 7.

10. The rest of the points of the HD-Grid can be obtained from the four eikonal simulations iterating step 5. For instance, to obtain A2 (see Figure 5) a vector within A1 and A4 is calculated and with the eikonal simulation it is possible to select the element that is at 4mm from A1.

Now that the HD-Grid is completely modeled, the framework also has to be able to retrieve the signals from the obtained points. The signal in point A1, that corresponds to a node in the mesh, is straightforward to retrieve, getting the EGM (calculated in step 1) from the node in the mesh. However, for the rest of the points that are inside of a mesh element, an interpolation within the nodes of those elements needs to be made. The first step is to transform the triangle element selected into an arbitrary one, using the matrix $B \in \mathbb{R}^{3x3}$. The explanation is again

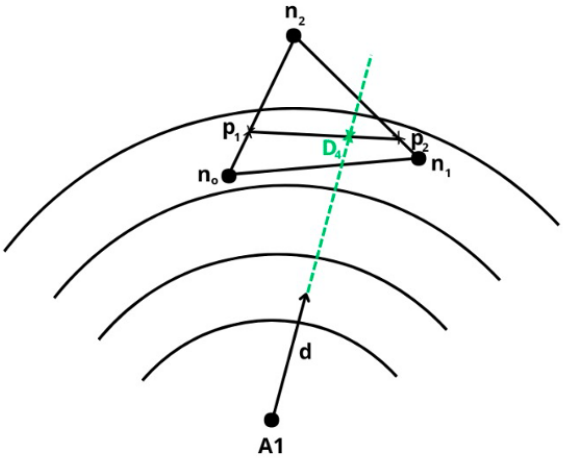

Figure 10: Process to obtain D4. The initialised vector is d, the nodes that define the elements are n_0, n_1 and n_2. The first step is to obtain p_1 and p_2 and then it is possible to obtain D4. The circumferential lines represent the isolines of the the eikonal simulation run from A1.

based on the same triangle of Figure 10, where each node has associated its cartesian coordinates (v_0, v_1 and v_2) and the value of its EGM (φ_0, φ_1 and φ_2). We need to transform the coordinates of D4 (named now p), into the coordidates of $\hat{p}$, which is the same point but on an arbitrary triangle (see Figure 11). We now that:

$$p = B\hat{p} + v_0 \tag{6}$$

So

$$\hat{p} = B^{-1}(p - v_0) \tag{7}$$

With $B = (v_1 - v_0, v_2 - v_0, (v_1 - v_0) \times (v_2 - v_0))$. Therefore, it is possible to obtain $\hat{p} = (\hat{p}_x, \hat{p}_y, \hat{p}_z)$. In the arbitrary triangle we have the following shape functions: $\hat{\Psi}_0 = 1 - \hat{x} - \hat{y}$, $\hat{\Psi}_1 = \hat{x}$ and $\hat{\Psi}_2 = \hat{y}$. Whith all of this, it is possible now to calculate $\varphi(p)$ as follows.

$$\varphi(p) = \varphi_0\hat{\Psi}_0(\hat{p}_x, \hat{p}_y, \hat{p}_z) + \varphi_1\hat{\Psi}_1(\hat{p}_x, \hat{p}_y, \hat{p}_z) + \varphi_2\hat{\Psi}_2(\hat{p}_x, \hat{p}_y, \hat{p}_z) \tag{8}$$

Taking the shape functions into consideration, and also the fact that the element is a 2D element and therefore has no component z, the Eq. 8 can be recasted into:

$$\varphi(p) = \varphi_0 + (\varphi_1 - \varphi_0)\hat{p}_x + (\varphi_2 - \varphi_0)\hat{p}_y \tag{9}$$

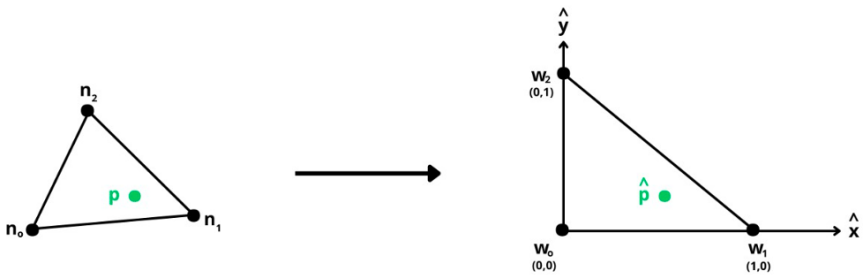

Figure 11: Transformation of the triangle on the left into an arbitrary one (on the right). This is done to get the value of the EGM in p

3.5 Bipolar EGMs and Propagation Map

The retrieved surface signals using the method of the previous section can be then analysed by computing bipolar EGMs, omnipolar EGMs, vector maps, the vector field heterogeneity and many other parameters. In this research, bipolar EGMs and vector maps were computed to study their validity and to show that they can be successfully extracted from the model we are using.

4 Results

Only by using the atrial coordinates of the starting point of the AP and the vetricular coordinates of its ending point, any AP can be introduced to the model. This can be seen in Figure 12, where the AP has been introduced in a random location.

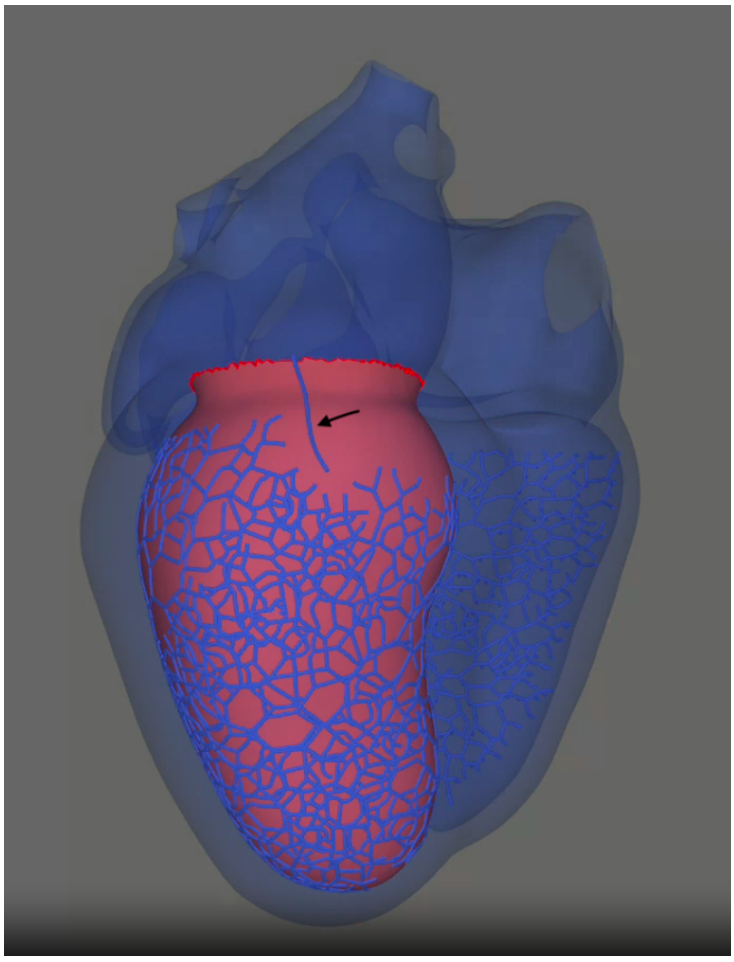

Figure 12: Representation of the AP in the heart model. The purkinje system can be seen (in blue) over the endocardial surface (in red) and the AP (in blue indicated with a black arrow) is a duct that connects the atria to the ventricles.

Once the pathway has been introduced, a complete heart depolarisation can be simulated taking the pathway into consideration, as shown in Figure 13.

The data generated on the simulation was retrieved with the HD-Grid model, as it was completely modeled as Figure 14A shows, successfully being able to calculate the points at the required distances from one another. Figures 14B and 14C show two different locations of the complete model of the heart with the AP and a location where the HD-Grid is placed.

With all this framework built up, the next great achievement is to retrieve the EGM unipolar signals from those points (Figure 15A). The bipolar signals can then be calculated from the

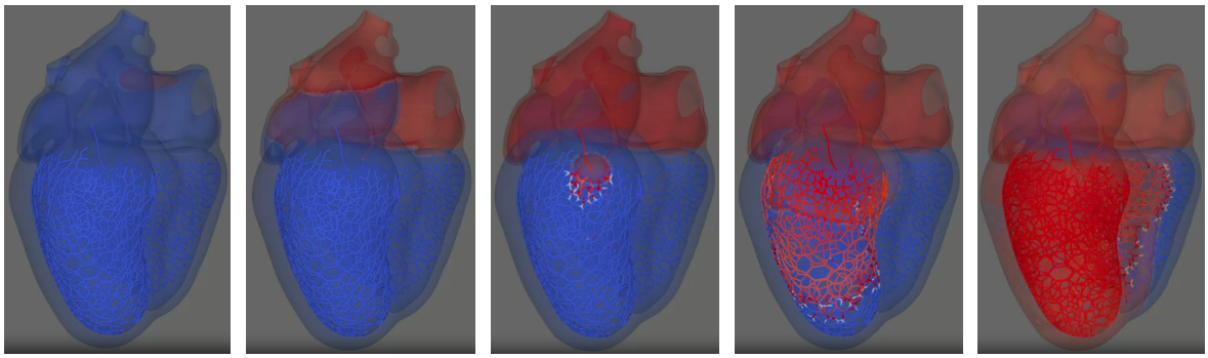

Figure 13: Series of frames that show the depolarisation of the heart taking into consideration the AP that has been introduced to the model.

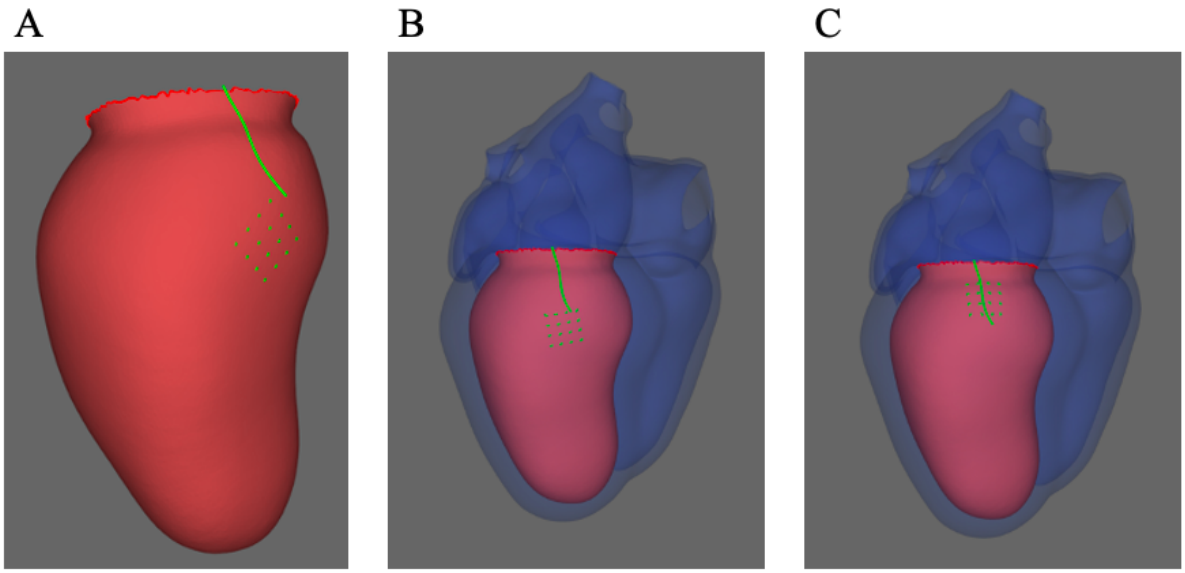

Figure 14: The read structure in A is the endocardial surface of the heart. The long thread in green is how an AP is modeled. The green points are the exact locations of the HD-Grid electrodes and where the EGMs are retrieved. B and C show the complete heart model with two different placement locations of the HD-Grid.

subtraction from two unipolars (Figure 15B). If compared with real signals, the bipolar EGMs look quite similar as Figure 15C shows. The symbol of the delflection should not be accounted because it is negative when the unipolar signal that subtracts to the other starts earlier and positive in the other case.

With the unipolar signals it is also possible to obtain parameters like the vectors -or propagation- maps (Figure 16).

5 Discussion

The method of constructing an HD-Grid virtual model developed in this research is going to help gain more knowledge about APs and how can they be localised. This research presents a detailed virtual model of cardiac electrophysiology representing an antegrade AP in the form of a short atrio-ventricular bypass tract in WPW syndrome. An HD-Grid catheter model is laid over the ventricular endocardial surface of the cardiac model to obtain EGMs near the AP ending point. This virtual tool has the potential to be a basis for further research not

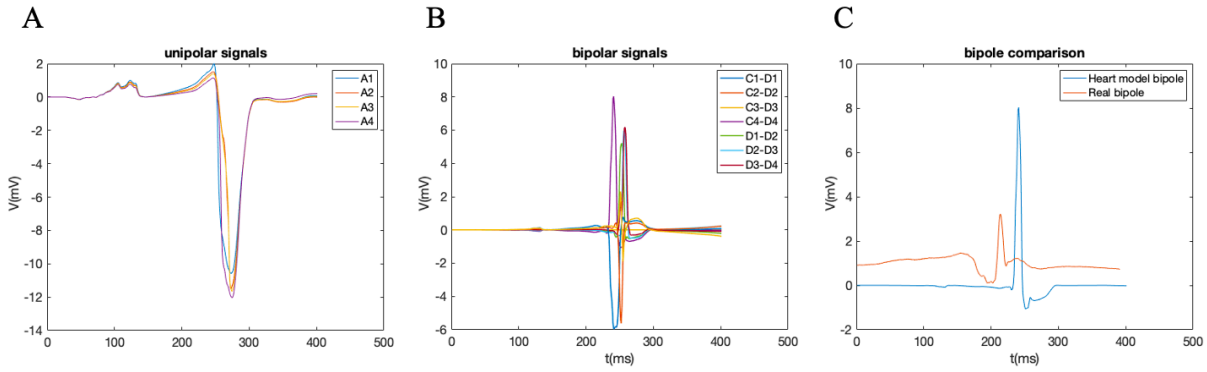

Figure 15: A shows the unipolar EGMs obtained from a random location of the modeled HD-Grid. B shows some of the bipolar EGMs calculated from the unipolars in A. C compares a real bipolar EGM (in orange) with one obtained in the model (in blue).

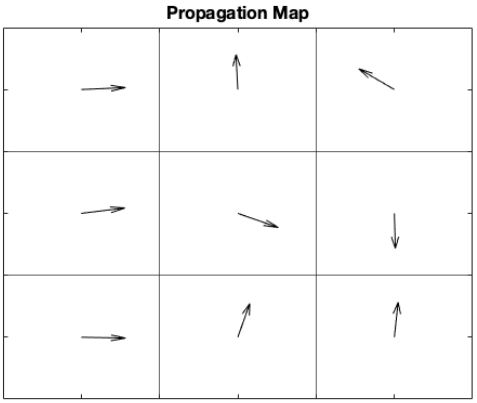

Figure 16: Vector map obtained form the unipolar signals retrieved from a random location of the HD-Grid model.

only in locating optimal ablation sites in patients with WPW syndrome, but also but also in enhancing the understanding of signals obtained during catheter mapping for other conditions, such as arrhythmias. Additionally, the procedures employed in constructing the HD-Grid model represent the first instance of extracting EGMs from a cardiac model utilising a catheter model. Furthermore, this methodology is versatile and can be applied to other high-density mapping catheters.

The extracted unipolar electrograms (EGMs) are employed to accurately compute bipolar EGMs, omnipolar EGMs, and vector maps. A comparative analysis between the computed bipolar EGMs and actual bipolar EGMs demonstrates a strong resemblance, suggesting that the model is effectively fulfilling its intended purpose. However, it can be detected from first sight that the modeled unipolar EGM signal is much stronger that the real data. This amplitude difference between the real bipolar EGM and the one extracted from the heart model could happen due to the fact that in real cases the contact between the heart's surface and the electrodes is not perfect and there will always be blood in between, decreasing the signal's amplitude. On the other hand, in our case, the electrodes are exactly within the surface, retrieving the highest possible amplitude. This can also be due to some parameters that can be changed in the model.

5.1 Limitations and Future Work

The results obtained in this research represent a base for future work regarding the AP localisation. However, there are also some limitations of this work that have to be assessed.

The first limitation is related with the heart models. Despite all their benefits, heart models still face some challenges. One significant issue is the complexity of accurately simulating the human heart's intricate structure and function. The heart's electrophysiological properties, mechanical behavior, and interaction with other body systems are extremely complex and not well understood nowadays, often requiring advanced computational techniques to model accurately.

Furthermore, there is limited knowledge about the actual topology of the HPS, its variability within the general human population, and the micro-anatomical structure of the purkinje ventricular junctions that couple the HPS with the myocardium [21]. It remains challenging to even characterize critical basic functional aspects of this system without invasive experiments, and these cannot capture HPS behavior on the organ level. Furthermore, selective destruction of the HPS can only be done once per heart, thereby severely limiting the amount of data collected [8]. During cardiac simulations, it was observed that the AP depolarised tissue, leading to retrograde conduction through the HPS, which caused depolarisation in other regions of the heart. This phenomenon can influence the activation times within the model, as areas distant from the AP may activate simultaneously with regions in close proximity due to HPS conduction. In the model employed, the HPS was extended to 90% of the distance to the heart's base, which may not accurately reflect physiological conditions across all patients or in children, as it remains uncertain to what extent the HPS extends towards the base of the heart

The Mitchell-Schaeffer ionic model represents another limitation. This model is a very simplified representation of the cellular membrane in a myocyte, replicating its behavior with only two membrane currents. While this may be enough for generating an electrophysiological depolarisation of the heart and producing a 12-lead ECG, it might not be adequate for accurately modeling real EGMs. Furthermore, usually WPW results in remodeling in the areas around the pathway. Therefore, a more sophisticated ionic model might be needed to model the syndrome.

Moreover, the APs can vary in shape and length, making it very difficult to model them. The example used in this research is a particular case, but this variation in the AP could lead to different outcomes on the simulations and on the analysed parameters.

Preliminary results suggest that the obtained signals are of high quality. However, future work involves a more extensive comparison with empirical data to validate the reliability and applicability of the computed signals. Further research will entail the goal for which the HD-Grid framework has been developed: finding a parameter that can be obtained during ablation procedures to guide cardiologists in accurately determining the ablation site in future interventions. To achieve so, different trials can be of interest, like simulating a complete reentry arrhythmia, where a single beat can lead to an electrical impulse going from atria to ventricles without pace. This can be interesting because for now, our model can only simulate one cardiac cycle. In addition to that, to better analyse the obtained parameters, different locations in the heart varying the pathway's position and length can be mapped.

The AP is modeled as an conductive fiber with a beginning point on the atria and an ending point on the ventricles. Therefore, although the HD-Grid framework has been developed for the ventricular endocardial surface, it could potentially be extended to the atrial endocardial surface to also identify the beginning point of the AP.

References

[1] Neic A, Gsell MA, Karabelas E, Prassl AJ, and Plank G. Automating image-based mesh generation and manipulation tasks in cardiac modeling workflows using meshtool. *SoftwareX*, 2020. 10

[2] Pappone C, Vicedomini G, Manguso F, Saviano M, Baldi M, and Pappone A et al. Wolff-parkinson-white syndrome in the era of catheter ablation: insights from a registry study of 2169 patients. *Circulation*, 2014. 2

[3] Wren C, Vogel M, Lord S, and et al. Accuracy of algorithms to predict accessory pathway location in children with wolff–parkinson–white syndrome. *Heart*, 2012. 2

[4] Lu CW, Wu MH, Chen HC, Kao FY, and Huang SK. Epidemiological profile of wolff–parkinson–white syndrome in a general population younger than 50 years of age in an era of radiofrequency catheter ablation. *International journal of cardiology*, 2014. 2

[5] Lu CW, Wu MH, Chen HC, Kao FY, and Huang SK. Epidemiological profile of wolff–parkinson–white syndrome in a general population younger than 50 years of age in an era of radiofrequency catheter ablation. *International journal of cardiology*, 2014. 2

[6] Lu CW, Wu MH, Chen HC, Kao FY, and Huang SK. Epidemiological profile of wolff-parkinson-white syndrome in a general population younger than 50 years of age in an era of radiofrequency catheter ablation. *Int J Cardiol*, 2014 Jul 1;174(3):530-4. 3

[7] de Groot N et al. Critical appraisal of technologies to assess electrical activity during atrial fibrillation: a position paper from the european heart rhythm association and european society of cardiology working group on ecardiology in collaboration with the heart rhythm society, asia pacific heart rhythm society, latin american heart rhythm society and computing in cardiology. *European Society of Cardiology*, 2022. 5

[8] Vigmond EJ and Stuyvers BD. Modeling our understanding of the his-purkinje system. *Progress in Biophysics and Molecular Biology*, 2016. 16

[9] Vigmond EJ, dos Santos RW, Prassl AJ, Deo M, and Plank G. Solvers for the cardiac bidomain equations. *Progress in Biophysics and Molecular Biology*, 2008. 9, 10

[10] Casado R et al. Characterization of accessory pathways using an orientation-independent catheter. *Clinical Electrophysiology*, 2018. 6

[11] Curtis DD et al. High-resolution, live, directional mapping. *Heart Rhythm*, 2020. 6

[12] Haissaguerre M et al. Electrogram patterns predictive of successful catheterablationofaccessorypathways. *Circulation*, 1991. 7

[13] Magtibay K et al. Reinserting physiology into cardiac mapping using omnipolar electrograms. *Cardicac Electrophysiology*, 2019. 6

[14] Shouvik KH et al. Resolving bipolar electrogram voltages during atrial fibrillation using omnipolar mapping. *Circulation Arrhythm Electrophysiology*, 2017. 6

[15] Sacher F, Wright M, Tedrow UB, O'Neill MD, Jais P, and Hocini M et al. Wolff–parkinson–white ablation after a prior failure: a 7-year multicentre experience. 2

[16] Hindricks G, Kojtkamp H, Chen X, Willems S, Haverkamp W, and Shenasa M. Localization and radiofrequency catheter ablation of left-sided accessory pathways during atria1 fibrillation. *Journals of the American College of Cardiology*, 1995. 5

[17] Plank G, Loewe A, Neic A, Augustin C, Huang YL, Gsell M, Karabelas E, Nothstein M, Prassl AJ, Sánchez Jand Seemann G, and Vigmond EJ. The opencarp simulation environment for cardiac electrophysiology. *Computer Methods and Programs in Biomedicine*, 2021. 10

[18] Bayer J, Prassl AJ, Pashaei A, Gomez JF, Frontera A, Neic A, Plank G, and Vigmond EJ. Universal ventricular coordinates: A generic framework for describing position within the heart and transferring data. *Medical Image Analysis*, 2018. 7, 8

[19] Gillette K, Gsell M, Kurath-Koller S, Prassl AJ, and Plank G. Exploring role of accessory pathway location in wolff-parkinson-white syndrome in a model of whole heart electrophysiology. *CinC abstract*, 2024. 2, 7, 8

[20] Gillette K, Gsell MA, Prassl AJ, Reiter U Karabelas E, Reiter G, Grandits T, Payer C, Stern D, Urschler M, Bayer J, Augustin Christoph, Neic A, Pock T, Vigmond E, and Plank G. A framework for the generation of digital twins of cardiac electrophysiology from clinical 12-leads ecgs. *Medical Image Analysis*, 2021. 7

[21] Gillette K, Gsell MA, Bouyssier J, Prassl AJ, Neic A, Vigmond EJ, and Plank G. Automated framework for the inclusion of a his–purkinje system in cardiac digital twins of ventric- ular electrophysiology. *Annals of biomedical engineering*, 2021. 7, 16

[22] Gillette K, Gsell MAF, Neic A, Manninger M, Scherr D, Roney CH, Strocchi M, Augustin CM, Prassl AJ, Vigmond EJ, and Plank G. A personalized real-time virtual model of whole heart electrophysiology. *Frontiers*, 2022. 7

[23] JP Keener. An eikonal-curvature equation for action potential propagation in myocardium. *Journal of Mathematical Biology*, 1991. 9

[24] Fananapazir L, German L, Gallagher J, Lowe J, and Prystowsky E. Importance of preexcited qrs morphology during induced atrial fibrillation to the diagnosis and localization of multiple accessory pathways. *Circulation*, 1990. 2

[25] El Hamriti M, Braun M, Molatta S, Khalaph M Imnadze G, Lucas P, and et al. Easy-wpw: a novel ecg-algorithm for easy and reliable localization of manifest accessory pathways in children and adults. *Europace*, 2023. 2

[26] Nguyen M, von Alvensleben JC, Runciman M, and Collins K. Advisor high-definition hd grid catheter for mapping accessory pathways in pediatrics. *Heart Rhythm Society*, 2020. 6

[27] Wierzbicki Mand Drangova M, Guiraudon G, and Peters T. Validation of dynamic heart models obtained using non-linear registration for virtual reality training, planning, and guidance of minimally invasive cardiac surgeries. *Medical Image Analysis*, 2004. 7

[28] Grider MH, Jessu R, and Kabir R. *Physiology, Action Potential*. StatPearls Publishing LLC, 2023. 3

[29] Schaeffer DG Mitchell CC. A two-current model for the dynamics of cardiac membrane. *Bulletin of mathematical biology*, 2003. 10

[30] Arruda MS, McClelland JH, Wang X, Beckman KJ, Widman LE, Gonzalez MD, and et al. Development and validation of an ecg algorithm for identifying accessory pathway ablation site in wolff-parkinson-white syndrome. *Journal of cardiovascular electrophysiology*, 1998. 2

[31] Prassl AJ Niederer SA Bishop MJ Vigmond EJ Plank G Neic A, Campos FO. Efficient computation of electro- grams and ecgs in human whole heart simulations using a reaction-eikonal model. *Journal of computational physics*, 2017. 9, 10

[32] Berenfeld O and Abboud S. Simulation of cardiac activity and the ecg using a heart model with a reaction-diffusion action potential. *Medical Engineering Physics*, 1996. 9

[33] School of Health Sciences. University of Nottingham. A beginners guide to normal heart function, sinus rhythm and common cardiac arrhythmias. 3

[34] Abbott Products and Innovation. Cardiac mapping: Changing the game with advisor hd grid. Technical report, Abbott, 2020. 5

[35] Meo M Dubois R Boyle PM Trayanova NA Cochet H Niederer SA Vigmond EJ Roney CH, Pashaei A. Uni- versal atrial coordinates applied to visualisation, registra- tion and construction of patient specific meshes. *Medical Image Analysis*, 2019. 7, 9

[36] Ruiperez-Campillo S, Pancorbo L, Ramirez E, Chorro FJ, Merino JL, Casado-Arroyo R, Castells F, and Millet J. Quantifying local cardiac substrate heterogeneity from high density recordings: an experimental study. *Europace 2024*. 6

[37] Niederer SA, Lumens J, and Trayanova NA. Computational models in cardiology. *Nature Reviews Cardiology*, 2019. 2

[38] Wellens HJ Sternick EB, Sanchez-Quintana D and Anderson RH. Mahaim revisited. *Arrhythmia Electrophysiology Review*, 2022. 9

[39] Pambrun T, El Bouazzaoui R, Combes N, Combes S, Sousa P, Le Bloa M, and et al. Maximal preexitation based algorithm for localization of manifest accessory pathways in adults. *JACC Clinical Electrophysiology*, 2018. 2

[40] The cardiac action potentials. 3

[41] Stevenson W.G and Soejima K. Recording techniques for clinical electrophysiology. *Journal of Cardiovascular Electrophysiology*, 2005. 4

[42] Chen X, Borggrefe M, Shenasa M, Haverkamp W, Hindricks G, and Breithardt G. Characteristics of local eiectrogram predicting successful transcatheter radiofrequency ablation of left-sided accessory pathways. *Journals of the American College of Cardiology*, 1992. 5